Supporting Information

Enhanced Charge Transfer Kinetics at Electrode/Electrolyte Interface in Acetonitrile Solvent for Lithium-ion Battery Cathodes

Tatsumi Suzuki, [a] Yuki Miyaura, [a] Ken-ichi Okazaki, [a] Chengchao Zhong, [a] Keiji Shimoda, [b] Fumiya Kondo, [c] Masanori Fujii, [c] Hajime Kinoshita [c] and Yuki Orikasa*[a]

[a] *Department of Applied Chemistry, Ritsumeikan University, 1-1-1 Nojihigashi, Kusatsu, Shiga 525-8577, Japan*
[b] *Ritsumeikan Global Innovation Research Organization, Ritsumeikan University, 1-1-1 Nojihigashi, Kusatsu, Shiga 525-8577, Japan*
[c] *KRI, Inc., 134 Chudoji Minami-machi, Shimogyo-ku, Kyoto 600-8813, Japan*

* Yuki Orikasa (orikasa@fc.ritsumei.ac.jp)

Table S1. Physical property data of acetonitrile and conventional carbonate-based solvents[S1, S2, S3].

Solvent	Viscosity (at 298 K) / mPa s	Donor Number
Ethylene carbonate (EC)	1.90 (at 313 K)[S1]	16.4[S1]
Propylene carbonate (PC)	2.50[S1]	15.1[S1]
Acetonitrile (AN)	0.37[S2]	14.1[S3]

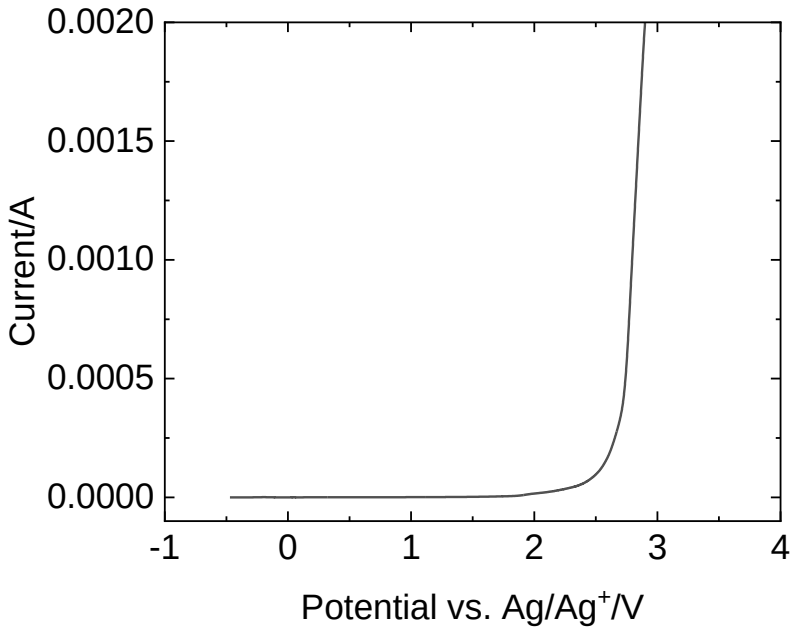

Figure S1. Linear sweep voltammogram of Pt electrode in 1 M LiTFSI/AN solution. Scan rate was set at 1 mV s^{-1} at room temperature. The oxidation stability of LiTFSI/AN is confirmed to be high up to 2.0 V vs. Ag/Ag^+. This potential corresponds to approximately 5.2 V in the Li/Li^+ reference[S4], indicating that decomposition of acetonitrile does not occur within the charge/discharge conditions used in this study.

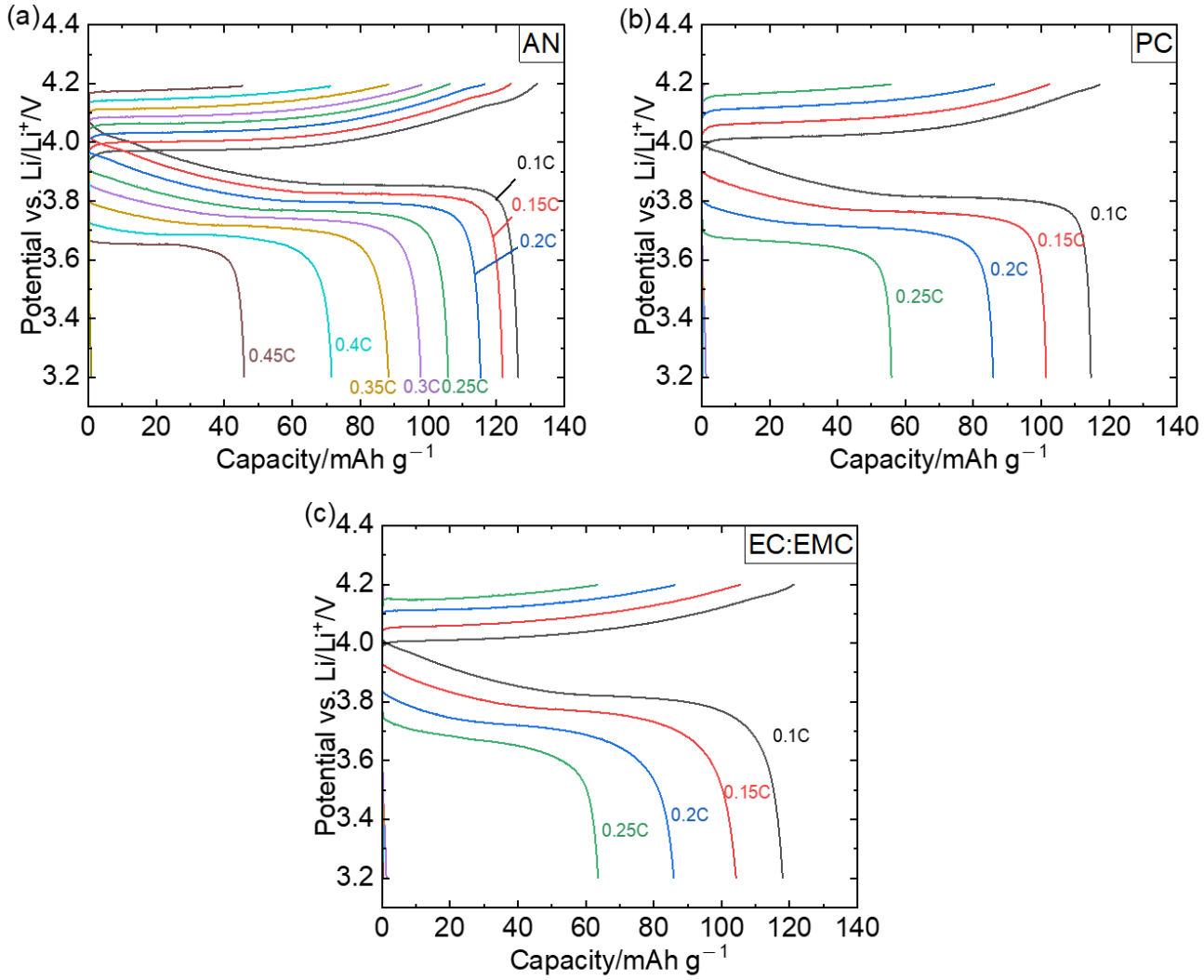

Figure S2. Charge/discharge profiles of the dual-compartment cells with LiCoO2 composite electrodes as the working electrodes and (a) AN, (b) PC, and (c) EC:EMC (3:7 v/v%) containing 1 M LiTFSI as the WE-side electrolytes at 298 K. All cells were cycled twice at each current rate within the potential range of 3.2-4.2 V, and second cycled data are shown here.

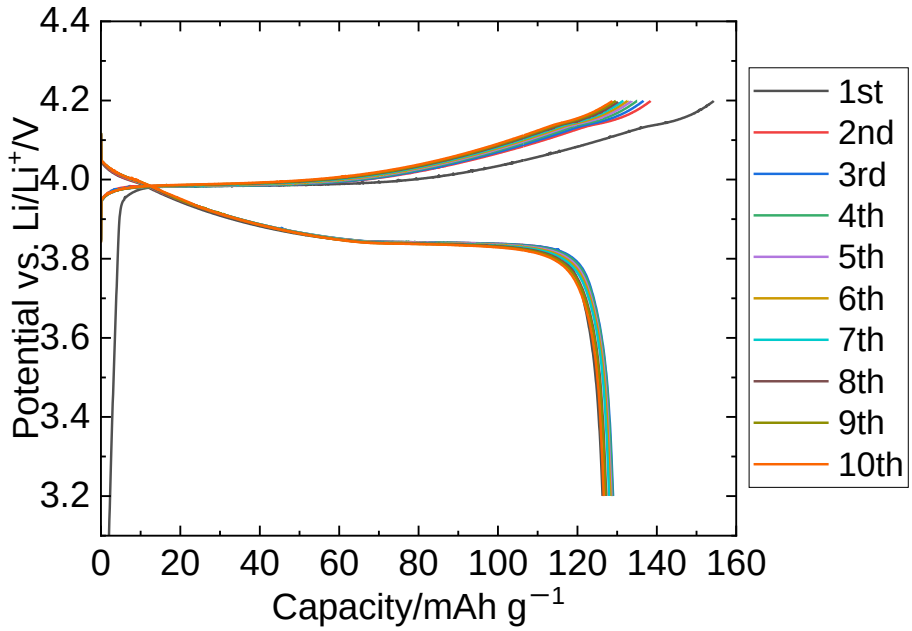

Figure S3. Charge/discharge cycle profiles of the dual-compartment cell with a $LiCoO_2$ composite electrode as the working electrode and AN containing 1 M LiTFSI as the WE-side electrolyte at the current rate of 0.1C at 298 K.

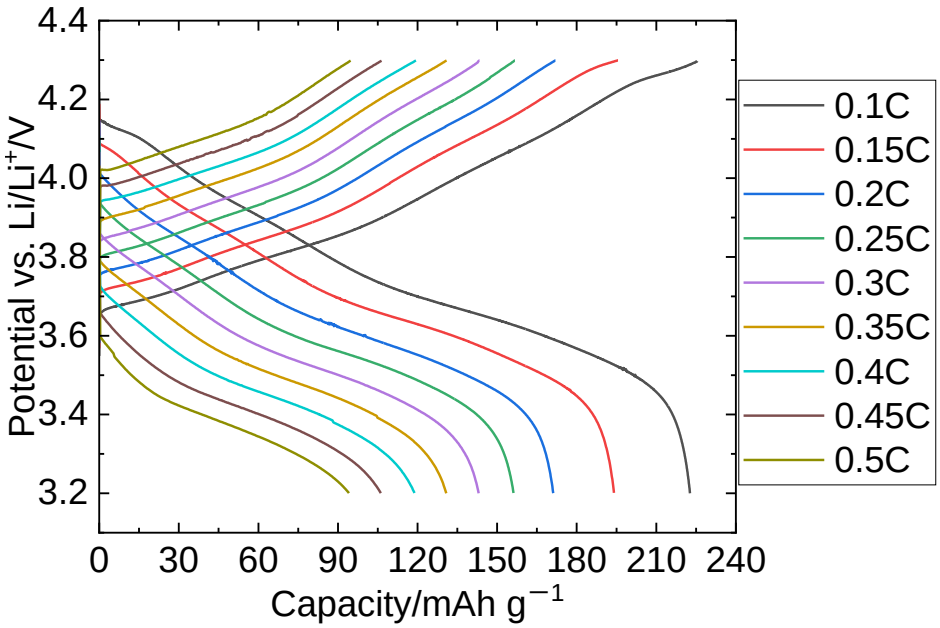

Figure S4. Charge/discharge profiles of the dual-compartment cell with a $LiNi_{0.8}Mn_{0.1}Co_{0.1}O_2$ composite electrode as the working electrode and AN containing 1 M LiTFSI as the WE-side electrolyte. The cell was cycled twice at each current rate within the potential range of 3.2-4.3 V vs. Li/Li^+ at 298 K, and second cycled data are shown here.

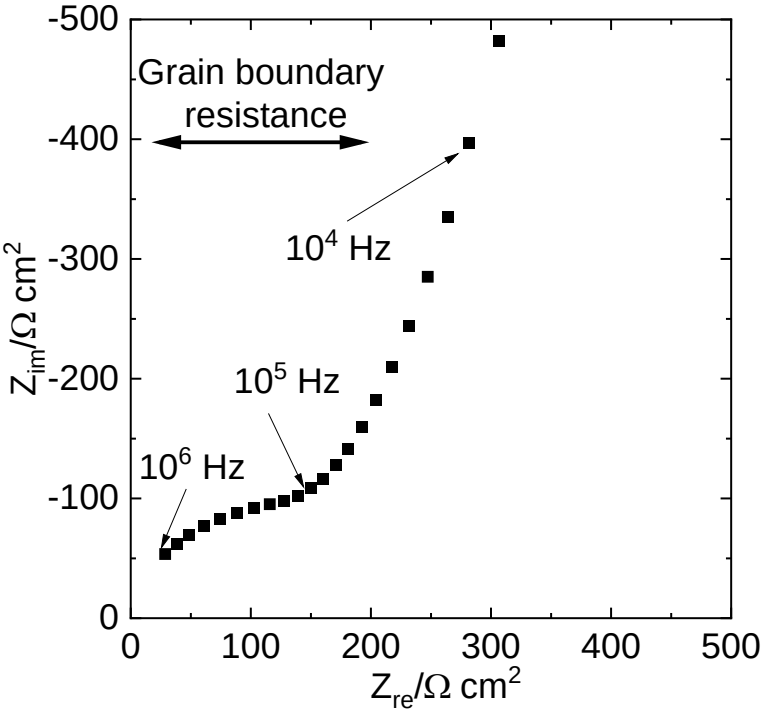

Figure S5. Nyquist plot of Au|LATP|Au cell at room temperature. The grain boundary resistance of LATP was observed in high frequency region above 10^4 Hz.

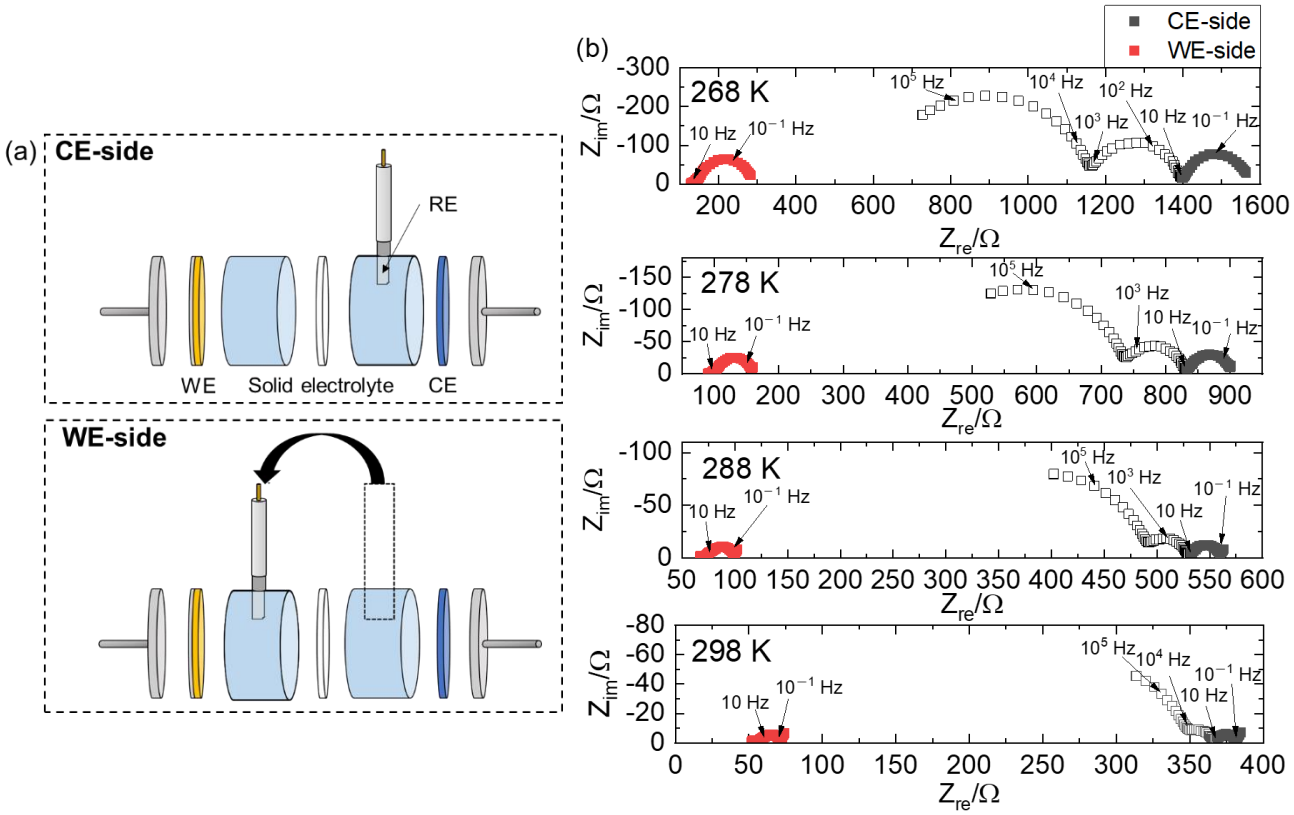

Figure S6. (a) Schematic illustration of the cell with the reference electrode placed in the CE-side (top) and WE-side compartments (bottom), and (b) typical Nyquist plots of $LiCoO_2$ composite electrode|PC containing 1 M $LiClO_4$|LATP|PC containing 1 M $LiClO_4$|Li cell with the reference electrode placed in different compartments at the WE potential of 4.0 V vs. Li/Li^+ (Frequency range: 200 kHz-10 mHz, amplitude**:** 10 mV). EIS was carried out by repositioning the reference electrode in the same cell inside an Ar-filled glove box. The black plots show the results of the cell with the CE-side reference electrode, while the red plots show the results of the cell with the WE-side reference electrode. The filled markers of the black plots with the low-frequency semicircle correspond to the semicircle observed in the cell with the WE-side reference electrode.

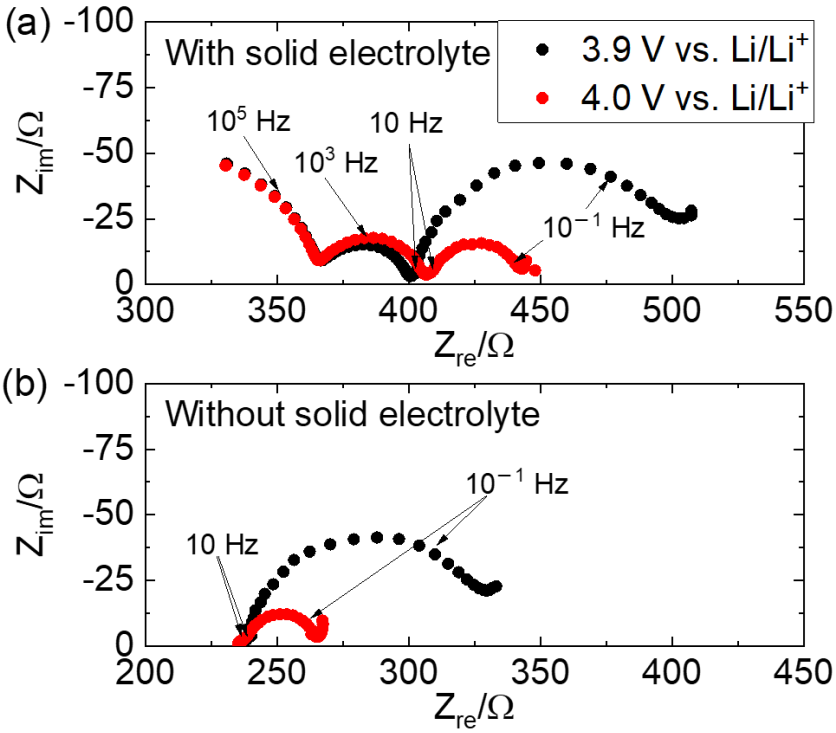

Figure S7. Comparison with Nyquist plots obtained from EIS for the cells with and without the solid electrolyte at room temperature. (a) $LiCoO_2$ composite electrode|PC containing 1 M $LiClO_4$|LATP|PC containing 1 M $LiClO_4$|Li, (b) $LiCoO_2$ composite electrode|PC containing 1 M $LiClO_4$|Li (Frequency range: 200 kHz-10 mHz, amplitude**:** 10 mV). The X-axis of each Nyquist plot shifted laterally because of the bulk resistance of the solid electrolyte ($R_{SE\text{-}bulk}$).

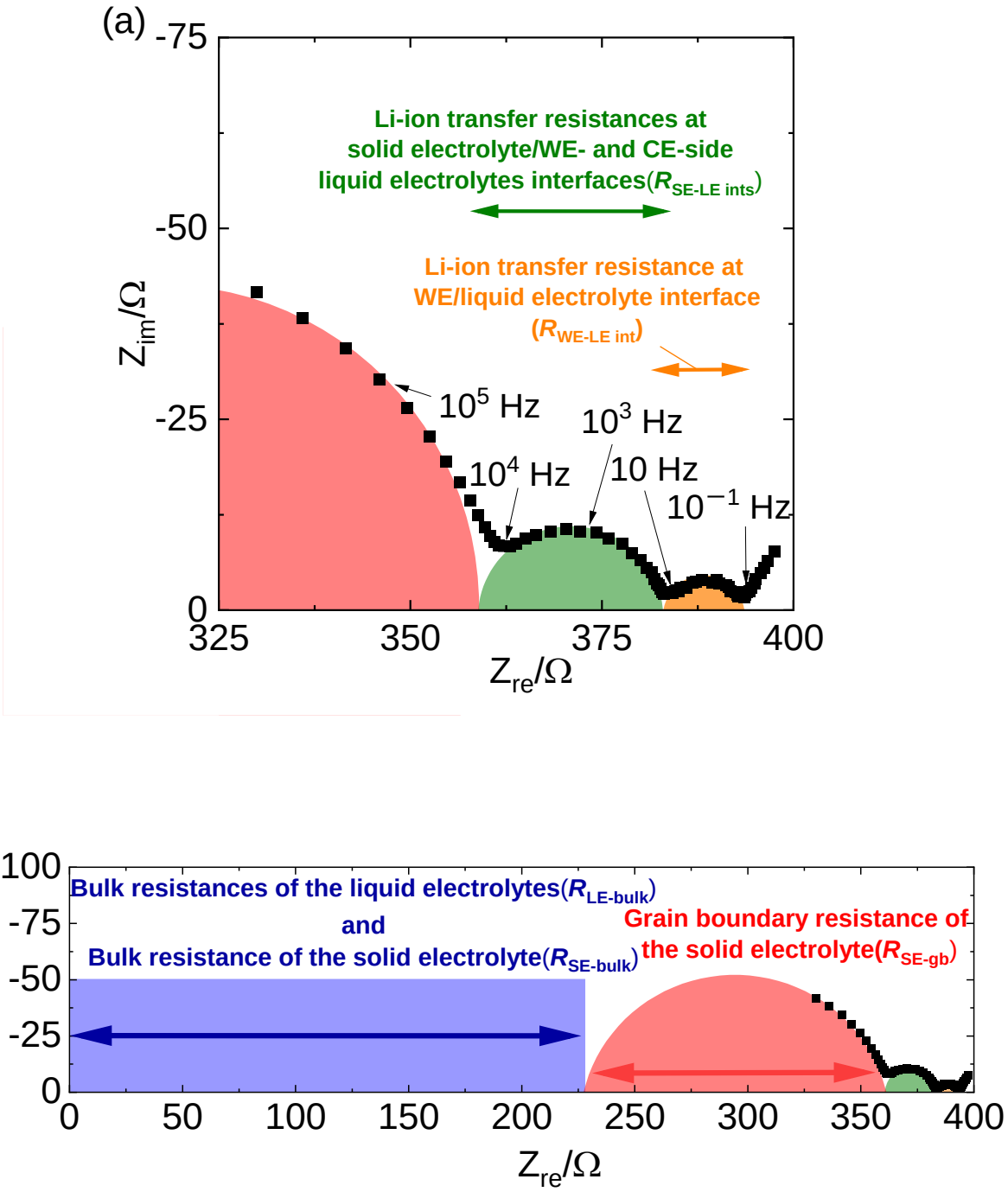

Figure S8. (a) Enlarged and (b) overall view of the typical Nyquist plots of the dual-compartment cell at the WE potential of 4.0 V vs. Li/Li^+ at 298 K (Frequency range: 200 kHz-10 mHz, amplitude: 10 mV). Note that the coloured semicircles are shown for visual guidance to help with assignment of resistance components.

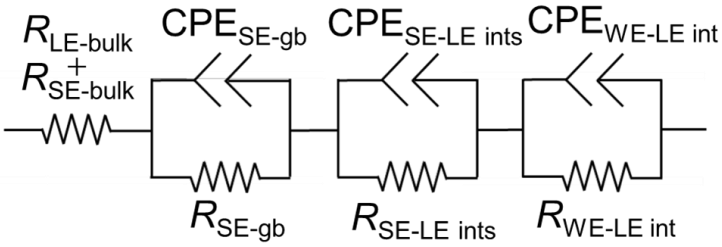

$R_{LE\text{-}bulk}$: Bulk resistances of the liquid electrolytes
$R_{SE\text{-}bulk}$: Bulk resistance of the solid electrolyte
$R_{SE\text{-}gb}$: Grain boundary resistance of the solid electrolyte
$R_{SE\text{-}LE\ int}$: Li-ion transfer resistances at solid electrolyte/WE- and CE-side liquid electrolytes interfaces
$R_{WE\text{-}LE\ int}$: Li-ion transfer resistance at WE/liquid electrolyte interface
CPEs : Constant phase elements

Figure S9. The equivalent circuit employed for fitting the experimental data.

Table S2. Resistance values obtained from EIS for the dual-compartment cells with each WE-side electrolyte. These resistance values were estimated by fitting using the equivalent circuit shown in Fig. S9.

Internal resistances	1 M LiTFSI/AN /Ω	1 M LiTFSI/PC /Ω	1 M LiTFSI/EC:EMC(3:7 v/v%) /Ω
Ohmic resistance ($R_{LE\text{-}bulk}$+$R_{SE\text{-}bulk}$)	98	227	168
$R_{SE\text{-}gb}$	128	136	144
$R_{SE\text{-}LE\ ints}$	13	20	22
$R_{WE\text{-}LE\ int}$	2	12	10

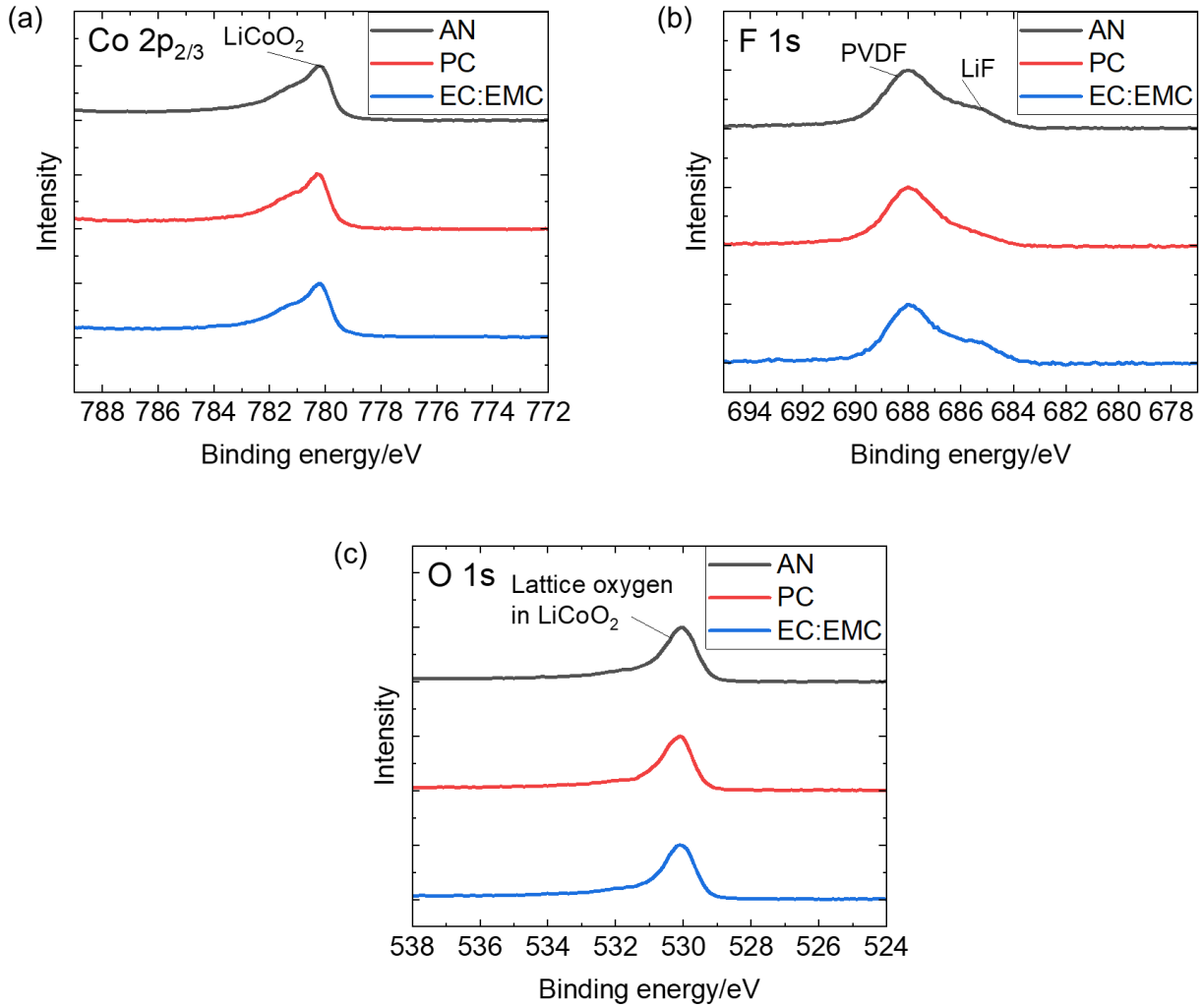

Figure S10. (a) Co $2p_{2/3}$, (b) F 1s, and (c) O 1s HAXPES spectra of the cycled $LiCoO_2$ composite electrodes in each WE-side electrolyte. Attributed species were also shown in Fig. S10: $LiCoO_2$[S5], PVDF[S5], LiF[S5, S6], and Lattice oxygen in $LiCoO_2$[S5]. Since the three WE-side solvents have sufficient anodic stability, cycling within the potential range of 3.2-4.2 V have resulted in the spectral peaks attributable to the oxidative decomposition of LiTFSI salt, rather than that of the solvents.

Table S3. The viscosities of three WE-side electrolytes in the temperature range of 268-298 K.

Temperature/K	1 M LiTFSI/AN /mPa s	1 M LiTFSI/PC /mPa s	1 M LiTFSI/EC:EMC(3:7 v/v%) /mPa s
268	2.03	33.3	11.8
273	1.73	24.5	9.79
278	1.55	21.2	8.27
283	1.41	16.9	7.17
288	1.38	15.0	6.63
293	1.31	12.9	5.89
298	1.27	11.3	5.43

References for Supporting Information

S1 M. Yoshio and A. Akiya, *J. Power Sources*, 1996, **62**, 219-222.

S2 K. Xu, *Chem. Rev.*, 2014, **114**, 11413-11862.

S3 P. Zhou, Y. Xiang and K. Liu, *Energy Environ. Sci.*, 2024, **17**, 8057-8077.

S4 Y. Marcus, *Pure Appl. Chem.*, 1985, **57**, 1129-1132.

S5 Y. C. Lu, A.N. Mansour, N. Yabuuchi and Y. Shao-Horn, *Chem. Mater.*, 2009, **21**, 4408-4424.

S6 J. N. Zhang, Q. Li, Y. Wang, J. Zheng, X. Yu and H. Li, *Energy Storage Mater.*, 2018, **14**, 1-7.